IEEE Access
Multidisciplinary | Rapid Review | Open Access Journal

Received 25 July 2022, accepted 11 August 2022, date of publication 17 August 2022, date of current version 23 August 2022.

Digital Object Identifier 10.1109/ACCESS.2022.3199367

RESEARCH ARTICLE

A Foldable Tightly Coupled Crossed Rings Antenna Array of Ultrawide Bandwidth and Dual Polarization

YANWEI FU[1], YONGWEI ZHANG[1], (Member, IEEE), QUAN SHI[1], MURAT TEMIZ[2], (Member, IEEE), AHMED EL-MAKADEMA[3], AND JIAJIA SHI[1], (Member, IEEE)

[1]School of Transportation, Nantong University, Nantong, Jiangsu 226019, China
[2]Department of Electronic and Electrical Engineering, University College London, London WC1E 7JE, U.K.
[3]Department of Electrical and Electronic Engineering, The University of Manchester, Manchester M13 9PL, U.K.

Corresponding author: Yongwei Zhang (david.y.zhang@ntu.edu.cn)

This work was supported in part by the NSFC under Grant 62174091, in part by the Postdoctoral International Exchange Program under Grant YJ20210098, in part by the Basic Science Research Program of Nantong City under Grant JC2020142, and in part by the Postgraduate Research and Practice Innovation Program of Jiangsu Province under Grant KYCX20-2792.

ABSTRACT Low-profile foldable array antennas are becoming increasingly more important for a wide range of applications such as satellite communications and wearable electronic devices. The conventional arrays formed by patch-like antennas have been extensively studied on surfaces with a curvature but they have exhibited limited bandwidth and polarization performance. This study investigates a coupling enhanced crossed rings antenna array with two typical configurations for dual polarization, which inherently produces ultrawide bandwidth, dipole-like polarization characteristics and a fully curved array (FCA) eventually. The fractional bandwidth of the array is over 100% on a planar surface and expanded to approximately 140% on the curved surface. For the bent array of slant polarization, the beamwidth increases by over 20° compared to the planar array and cross polarization discrimination (XPD) maintains above 15 dB. The effects of curvature on the impedance matching and polarized radiation patterns for such arrays are investigated by measuring the performance of the fabricated prototype arrays. The results revealed that the tightly coupled crossed rings antenna array on a curved surface has a potential to form multiple beams on a limited aperture size through smaller subarrays which can yield ultrawide bandwidth due to concentrated mutual coupling mechanism. This characteristic is promising in applications where traditional flat panel arrays are difficult to implement such as in mobile stations, moving platforms and for satellite communication on-the-move.

INDEX TERMS Cylindrical arrays, foldable arrays, phased arrays, tightly coupled dipoles.

I. INTRODUCTION

Electronically beam steered antenna arrays are becoming increasingly more important for various wireless communication systems such as satellite communication on-the-move (SOTM) and mobile communication systems [1], [2], [3], [4], [5], [6]. Unlike mechanically steered arrays, electronically steered arrays allow fast tracking of satellites with multiple beams while avoiding the use of bulky moving parts and offering great flexibility in terms of cost and performance. However, traditional flat panel arrays might be difficult to install on moving platforms particularly if certain aerodynamic features are required, such as aeroplanes, cars and trains, or for aesthetic purposes. For example, in order to receive low earth orbit (LEO) satellite signals, electronic scanned antenna arrays of flat panels are not sufficient, mechanical maneuver is often required for azimuthal scanning [3]. Hence, flexible antenna array as an effective solution that can conform to versatile carrier profiles while producing a wide field of view is desired.

The associate editor coordinating the review of this manuscript and approving it for publication was Jenny Mahoney.

Phased antenna array (PAA) with full electronic beam steering capability may be the only emerging solution for SOTM, which can conform to the shape of the moving platform. Hence, it is very attractive for mobile ground-to-satellite service antennas as it can offer extremely low-profile and beam pointing agility [7]. Since the first experiment to realize communications and position-fixing on automotive vehicles using satellites by R. Anderson *et al*. in 1981 [8], there have been continuous efforts to develop the technology further to realize more advanced features such as multibeam steering, polarization control. Furthermore, large efforts have been made to reduce the profile of the phased arrays in order to allow better integration with the platform to provide more flexibility [9]. One of the key challenges for the technology to be deployed in practice is the limited scan range. For flat based planar arrays, the maximum scan angle is typically within the range of $\pm 60^\circ$ off boresight [10], [11]. On the other hand, an antenna arrays made from flexible material can potentially yield an extended scan range while providing better adaptability to the surface shape of required platform.

Patch-type antennas have been favorable structures to form low-profile foldable arrays [12], [13], [14]. The arrays of patch antennas or microstrip antennas and Vivaldi antenna on cylindrical surfaces have been widely studied for a variety of applications [15], [16], [17]. However, this category of the antenna has many inherent disadvantages such as narrow bandwidth, poor polarization purity, spurious feed and radiation pattern characteristic. On the other hand, antennas of balanced structure such as a dipole have the potential for better polarization performance and broad bandwidth making them better candidates for the design of high performance phased arrays. Tightly coupled dipole arrays formed on cylindrical surfaces were studied in [18] where horizontally omni coverage was the main concern. However, the effect of curvature on the tightly coupled dipole arrays have not been extensively studied before, in particular for arrays of dual polarization.

Tightly coupled dipole arrays (TCDA) have demonstrated broad bandwidth characteristics, high polarization purity, and low profile. However, the total height of the array is constrained by the separation between the array elements and the ground plane [19], [20]. The minimum height of TCDA was reported as slightly shorter than a quarter wavelength of the highest operational frequency [21], [22]. Based on the initial concept presented by Munk [23], capacitive coupling is introduced between the antenna elements to counter the inductive effect of the ground plane at low frequencies. The tip-end capacitance in the dipole array increases the frequency bandwidth to a certain degree, but not sufficiently wide enough, especially when the array needs to scan a large angle off the broadside. The conventional solution to this problem is to utilize wide-angle impedance matching (WAIM) structures made up of a stack of dielectric layers on top of the antenna array surface. More recently, metasurfaces or frequency selective surfaces (FSS) have been used to increase frequency bandwidth and scan range. The design of these structures increases the complexity of the project.

Wide-angle scanning is critical for antenna arrays to be used in practice on moving platforms such as on ground terminals in SOTM application. The characteristics of the antenna arrays are closely related to the profile of the array and its physical dimensions. Bending the antenna array has an potential impact on the input impedance characteristic, radiation patterns and scan performance. It is reported in [24] that the maximum scan angle can be increased from 50° to more than 90° by placing a linear array on a cylindrical surface and the scan range for the bent antenna array can be significantly improved by an appropriate choice of the array bending angle. In [25], a narrowing of multibeam positions and a broader frequency range were observed in the rectangular waveguides array on the curved geometry as compared to a planar array. Reflection coefficient and radiation patterns of different antennas due to bending were investigated in [26], [27], [28], [29], and [30]. However, the characteristics of ultrawideband arrays like TCDA on curved surface need more investigation.

The antenna elements for TCDA type of arrays are inherently balanced structures that require the feeding network with a balanced structure and a function of impedance matching. However, common-mode resonances may occur when the balanced feeding lines are present between the surface of the array and the ground plane [31]. There are a variety of feeding methods including inserting Balanced-Unbalanced structures to feed such arrays [32], [33], [34]. However, integration of wideband balun between the array surface and the ground plane significantly increases the design complexity. Therefore, a simpler method is desired to feed the array element of a balanced structure while providing a single-ended port for termination. A bent Coplanar Waveguide (CPW) formed on a thin substrate was used to feed the crossed disk antenna element while transforming the characteristic input impedance to 50 Ohms for verification measurements [35]. Due to the flexible substrate, CPW is used easily as feedline in conformal antenna array.

In this study, finite arrays based on tightly coupled crossed disk arrays were investigated under two typical antenna array configurations. They were formed on a planar or a convex surface with Horizontal/Vertical(*H/V*) and $\pm 45^\circ$ polarization, respectively. The electromagnetic performance of the finite arrays on two types of surfaces was compared incorporating two different polarization orientations in each case. The capabilities of finite arrays formed by tightly coupled disks including ultrawide bandwidth, wide scan range, and dual polarization were examined considering the effect of curvature.

II. ULTRAWIDEBAND ANTENNA ARRAY DESIGNS

A. SCAN IMPEDANCE ANALYSIS

For a tightly coupled dipole array, mutual coupling plays a crucial role to achieve broad bandwidth. The induced-emf (electromotive force) method can be used to study the mutual impedances in the arrays. Two different configurations of dipole arrays are illustrated in Fig. 1, where three elements are

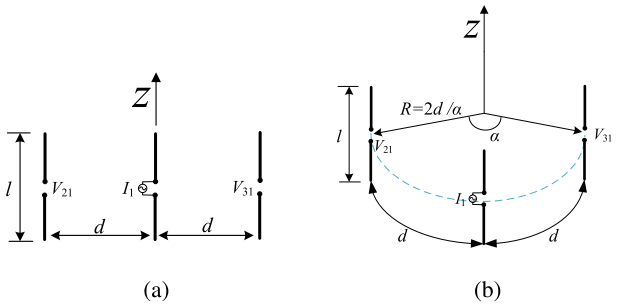

FIGURE 1. Scan impedance analysis of the arrays based on two different configurations. (a) Linear array where the element number is 2, 1, and 3 from left to right. (b) Bent array where the radius of circle for bending is $R=2d/\alpha$ and the element 1 is in the front.

arranged in a linear and curved configuration, respectively. Based on the hypothesis of sinusoidal current distribution in the linear radiators, the self-impedance of parallel line antennas with length l can be calculated by [36]

$$R_m = \frac{\eta}{2\pi}\{C + \ln(kl) - C_i(kl) + \frac{1}{2}\sin(kl)\,[S_i(2kl) - 2S_i(kl)] + \frac{1}{2}\cos(kl)\,[C + \ln(kl/2) + C_i(2kl) - 2C_i(kl)]\}, \quad (1)$$

$$X_m = \frac{\eta}{4\pi}\left\{2S_i(kl) + \cos(kl)\,[2S_i(kl) - S_i(2kl)] - \sin(kl)\,[2C_i(kl) - C_i(2kl) - C_i(\frac{2ka^2}{l})]\right\}, \quad (2)$$

where $C = 0.5772$, $S_i(x)$ and $C_i(x)$ are the sine and cosine integral functions, and a is the radius for the dipole. The mutual impedance of two parallel dipole antennas with distance d at feed points where the current is assumed at its maximum can be derived by

$$R_{21} = \frac{\eta}{4\pi}\,[2C_i(u_0) - C_i(u_1) - C_i(u_2)], \quad (3)$$

$$X_{21} = -\frac{\eta}{4\pi}\,[2S_i(u_0) - S_i(u_1) - S_i(u_2)], \quad (4)$$

$$u_0 = kd, \quad (5)$$

$$u_1 = k\left(\sqrt{d^2 + l^2} + l\right), \quad (6)$$

$$u_2 = k\left(\sqrt{d^2 + l^2} - l\right). \quad (7)$$

The scan impedance of the center element for both configurations have been calculated using the induced-emf method and a full-wave simulator. With the following setting: l = 60 mm, d = 60 mm, a = 0.004 mm, and g = 0.4 mm that is the gap for the feed at the center of the dipole in the full-wave simulation, the derivation of scan impedance for the center element presented in Fig. 1 is summarized in Table 1. The analytic results were calculated based on the emf-method, where $Z_1 = Z_{11}+Z_{21}+Z_{31}$, and $Z_{31} = Z_{21}$ in both the planar and bent configurations. The spacing between two adjacent elements changed from 0.5λ in the planar case to 0.487λ ($\alpha = \pi$) and 0.45λ ($\alpha = \pi/2$) in the bent configuration. Variations in the mutual impedance were observed between the three

TABLE 1. Scan impedance of the center element of dipole antenna array of three elements at 2.5 GHz on a planar and curved surface, l = 60 mm, when d = 60 mm, a = 0.004 mm, and g = 0.4 mm is the gap at the center of the dipole for feed.

Number of	Z_{11}		Z_{21}		Z_1	
element	emf	full-wave	emf	full-wave	emf	full-wave
1	73+42j	80+45j	NA	NA	NA	NA
3 (planar)	73+42j	84+49j	-13-30j	-18-32j	47-18j	48-15j
3 (bent $\pi/2$)	73+42j	84+50j	-10-31j	-16-34j	53-20j	52-18j
3 (bent π)	73+42j	84+51j	-4-35j	-9-38j	65-28j	66-25j

scenarios as the relative separation between elements were changed. It was observed that mutual impedance is significant to determine the scan impedance of the centre element in both configurations, and it is more dominant when the spacing between the elements is smaller. The active reflection coefficient of the elements in an array has the following relationship with the scan impedance

$$\Gamma_{act} = \frac{Z_1 - Z_0}{Z_1 + Z_0}, \quad (8)$$

where Z_1 is the scan impedance of the elements in the array, and Z_0 is the characteristic impedance of the transmission line connected to the array elements. With the arch length equal to the length of the planar array (i.e., $2d$), the arrays formed on the curved surface with the bending angle of $\alpha = \pi/2$ and $\alpha = \pi$, the active reflection coefficient is −10.6 dB, −11.4 dB and −13.9 dB for the center element under the three scenarios (three elements in a line, on curved surface with $\alpha = \pi/2$ and $\alpha = \pi$, and Z_0 = 84 Ω). The corresponding VSWR (voltage standing wave ratio) is 1.8, 1.7, and 1.5, respectively.

On the other hand, the active reflection coefficient of an element in an antenna array can also be derived by scattering parameters of the array and this is presented in Subsection D. The induced-emf method helps analytically interpret the coupling mechanism in half-wavelength antenna arrays, but for a tightly coupled dipole array of ultrawide antennas, scattering parameters is more convenient for modelling the coupling as the analytical model becomes invalid.

B. ANTENNA ARRAYS ON CURVED GEOMETRY

The geometry of conformal array antennas with the two typical polarization schemes is illustrated in Fig. 2. The finite array shown in Fig. 2a consists of four elements positioned in the horizontal planes with four rows of them in the vertical direction, the radius of the cylinder is R and a is the arch length between the adjacent elements in the horizontal plane. The array element is assumed a dipole with *H/V* polarization. Therefore the arc length of the conformal array is $4a$ which makes the total angle of the arch in the horizontal plane $\alpha_a = 4a/R$. The element for the finite array in Fig. 2b is a dipole but with ±45° polarization. The separation distance between the adjacent elements in the direction of ±45° remains a, then the total angle of the arch in the horizontal plane is $\alpha_b = 4\sqrt{2}a/R$.

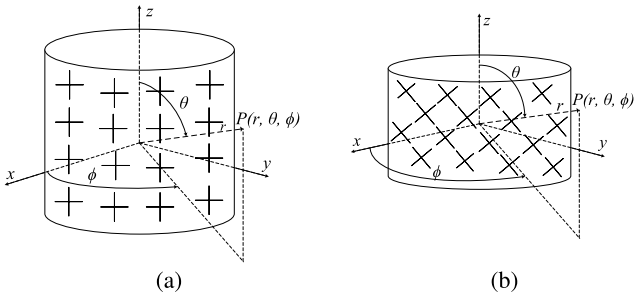

FIGURE 2. Cylindrical array geometry and dual polarization schemes. (a) Coordinate system for dipole elements of *H/V* polarization. (b) Coordinate system for dipole elements of slant polarization.

The arrays in Fig. 2a, 2b can also be considered as 4- and 2-element subarrays, respectively. The subarrays are vertically placed with equal spacings of a and $\sqrt{2}a$ respectively, however with an alternate offset horizontally in the latter case. The position vector of each element can be specified by their coordinate. The azimuth coordinates of the elements in the mth subarray (m = 1, 2, . . . ,4 for the *H/V* polarization case and m = 1, 2 for the case of slant polarization) is given by

$$\boldsymbol{\alpha}_m = -0.5\alpha + ([1:N] - 0.5)\alpha/N + \pi/2, \tag{9}$$

where $\alpha = \alpha_a$ and $N = 4$ in Fig. 2a and $\alpha = \alpha_b$ and $N = 8$ in Fig. 2b. The arrays become symmetrical with respect to y-axis in the case of (9). The position matrix representing coordinates of elements in each subarray can be expressed as

$$\boldsymbol{R}_m = \begin{bmatrix} R\cos\boldsymbol{\alpha}_m \\ R\sin\boldsymbol{\alpha}_m \\ \boldsymbol{z}_m \end{bmatrix}, \tag{10}$$

where vector $\boldsymbol{\alpha}_m$ is given by (9) and $\boldsymbol{z}_m$ is the coordinates of the element in the mth subarray. For different subarray, $\boldsymbol{z}_m$ is consistent with the arithmetic sequence, the increment step is a and $\sqrt{2}a$ for the two array configurations shown in Fig. 2a and Fig. 2b respectively.

The array factor (AF) describes the spatial response of the all array elements. Considering the beam steering, AF of the finite array is given by [37]

$$AF = \sum_{i}^{N} a_i e^{jk\boldsymbol{r}_i\cdot\hat{\boldsymbol{r}}} e^{jk\boldsymbol{r}_i\cdot\hat{\boldsymbol{r}}_0}, \tag{11}$$

where a_i is the amplitude of the ith element which is assumed to be uniform, and $\hat{\boldsymbol{r}}$ is the spatial unit vector of the observation point $P(r, \theta, \phi)$, ϕ is the azimuth angle, and θ is the elevation angle, and $\hat{\boldsymbol{r}}_0$ is the unit scan vector that corresponds to the angle in space to which the main beam of the array is being steered.

The array elements were initially assumed dipoles where the element pattern is close to the shape of a cosine function. However, unlike the traditional element pattern in a planar array, the normal of each array element is oriented in a different direction in a conformal array. In the finite array, each element is pointing outward to the normal direction at

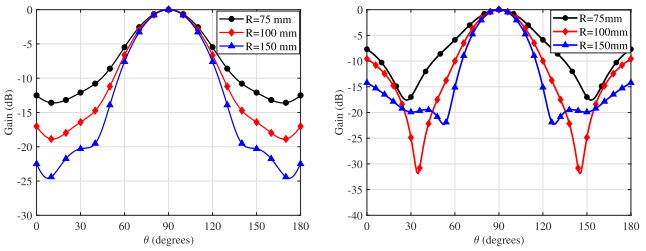

FIGURE 3. Calculated radiation patterns at 2.5 GHz for the conformal array that consists of 16 elements for elevation steering angle $\theta = 90°$ and azimuth steering angle $\phi = 90°$, corresponding to the radius of the cylinder for the curved surface. (a) The spacing between the adjacent elements in the horizontal and vertical plane is 40 mm. (b) The spacing between the adjacent elements in the horizontal and vertical plane is $40/\sqrt{2}$ mm.

the element position, not aligned to a same direction as in a planar array. The element pattern (EP) can be defined by

$$EP(\theta, \phi) = (\hat{\boldsymbol{n}}_i, \hat{\boldsymbol{r}}), \tag{12}$$

where

$$\hat{\boldsymbol{n}}_i = \frac{\boldsymbol{r}_i}{|\boldsymbol{r}_i|}, \tag{13}$$

and $\hat{\boldsymbol{n}}_i$ is the normal vector for the ith element position, and the element radiation pattern follows a cosine function. Intuitively, the element pattern is dependent on its position with respect to the angle of the observation, and when observing from the normal direction of the element position, the pattern follows a cosine function. Moreover, the synthesized array pattern is then calculated by,

$$F(\theta) = EP \cdot AF. \tag{14}$$

For the elements arranged in the geometries shown in Fig. 2, the radiation patterns of the finite arrays of two dual-polarized schemes are shown in Fig. 3. As expected, the beamwidth of the main lobe increases as the radius of the cylinder decreases. A narrower beam is observed for the slant polarized array with the same radius as the *H/V* polarization case. The performance of the finite array based on the dipole element for the two configurations shown in Fig. 2 and it is summarized in Table 2. However, arrays based on dipole elements are operating with a limited bandwidth, a dual-polarized element of ultrawide bandwidth is desired and proposed in the following section.

C. BROADBAND ELEMENTS AND ARRAY DESIGNS

Tightly coupled crossed disk antenna array demonstrates ultrawideband characteristics while maintaining physically a 2-D shape for each layer consisted in the array, which makes it suitable to be implemented on a curved surface. The unit cell of the proposed dual-polarized antenna is shown in Fig. 4. The array structure comprises three layers. The radiator layer of the array in the middle is formed by crossed disk dipoles. Capacitors were added between adjacent elements to counteract the inductive effect from the ground plane at

TABLE 2. Performance of finite dipole arrays on cylindrical surfaces.

Parameter	R =75 mm		R = 100 mm		R = 150 mm	
	H/V pol	slant pol	*H/V* pol	slant pol	*H/V* pol	slant pol
Beamwidth(^{o})	44	40	40	33	40	29
Gain (dB)	21.7	19.8	22.7	21.7	23.4	23

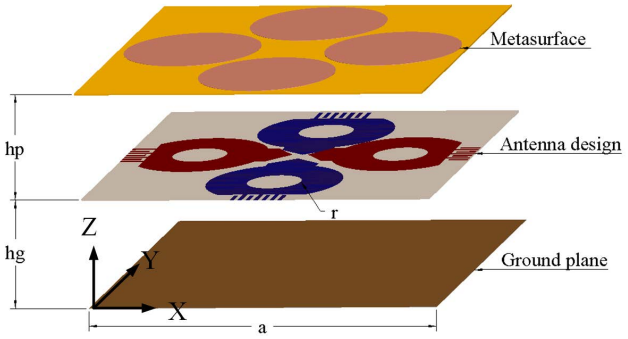

FIGURE 4. Unit cell design for the arrays of ultrawide bandwidth.

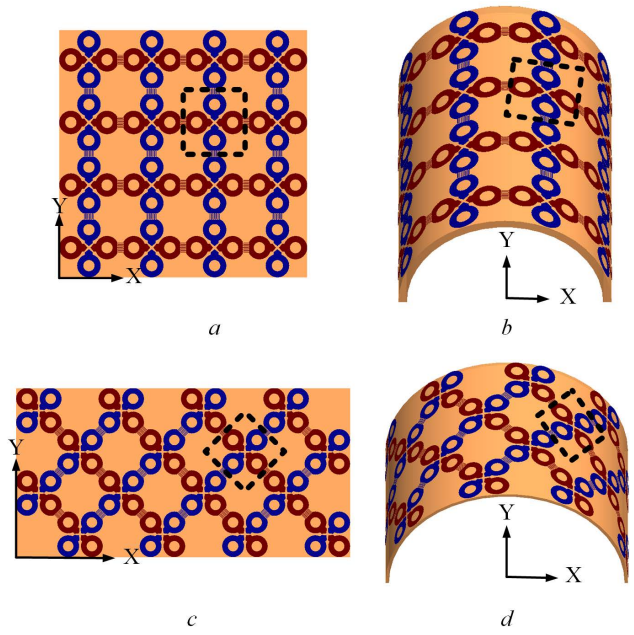

FIGURE 5. Aperture configurations of the finite antenna arrays. (a) Planar array configuration of 4 × 4 array with *H/V* polarization. (b) Bent array configuration of 4 × 4 array with *H/V* polarization. (c) Planar array configuration of 4 × 4 array with slant polarization. (d) Bent array configuration of 4 × 4 array with slant polarization.

the low frequency. Moreover, a metasurface layer formed by conductive disks was placed above the crossed disk dipole array with a distance of *hp* and the distance between the array surface and the ground plane is *hg*. Fig.5 illustrated the 4 × 4 array with *H/V* polarization and slant polarization on a planar surface and on a curved surface with a bending angle of 180° along the *y*- axis respectively. The elements for different polarization are marked in two different colours in both cases.

TABLE 3. Unit cell parameters for arrays of different frequency bands.

Freq	a (mm)	r(mm)	hg (mm)	hp (mm)	cap (pF)
1.5-7.3 GHz (131.8 %)	26	5	16	7	0.24
0.9-4.0 GHz (126.5%)	40	7.5	29	13	0.35
0.38-1.6 GHz (123.2%)	105	20	71.5	39.5	1

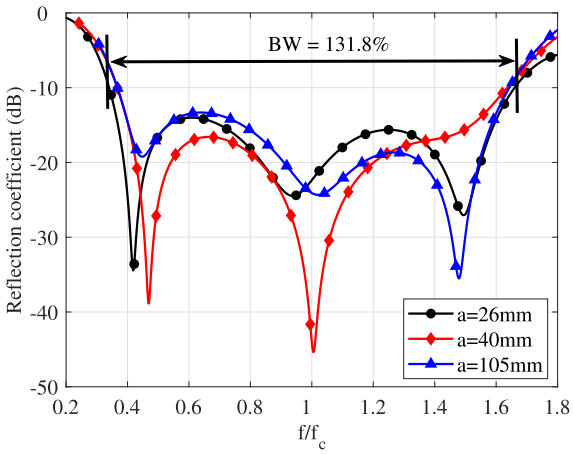

FIGURE 6. Frequency bandwidth of the tightly coupled crossed disk array antenna, the frequency band of operation depends on the element spacing and other parameters, the center frequency is 1 GHz, 2.45 GHz, or 4.4 GHz with the element spacing of a = 105 mm, 40 mm or 26 mm respectively, the corresponding capacitance between the adjacent elements is 1 pF, 0.35 pF, or 0.24 pF.

The coupling enhanced crossed ring antenna array is based on elements of a balanced structure and demonstrates ultra-wideband capability. The optimal dimensions of the infinite array operating at different frequency bands are given in Table 3. The reflection coefficients with respect to the element spacing for the infinite planar array operating at three frequency bands are given in Figure. 6. The ultrawideband capability of the array design is shown at different operational frequency bands and it is a scalable design with only few parameters to be optimized. It is a balanced structure, therefore an ultrawide bandwidth can be obtained with enhanced coupling between adjacent elements. This distinguishes the study from the other previous work where patch-like antenna structures were proposed and investigated previously in the literature.

D. PERFORMANCE OF THE FINITE ARRAYS

In a tightly coupled array, the mutual coupling is utilized on purpose to achieve a stable active impedance and radiation pattern over a broad frequency range, and a sinusoidal current distribution has to be maintained at each frequency. Since the size of each element is approximately half-wavelength ($\lambda/2$) of the highest frequency in the band, its size is too small to operate at the lower frequency end. Therefore, at the low frequency mutual coupling is critical to obtain the desired current distribution. Mutual coupling between the elements on a curved surface is expected to be different compared to the case on a planar surface. Mutual coupling between the centre element and the surrounding elements of the same

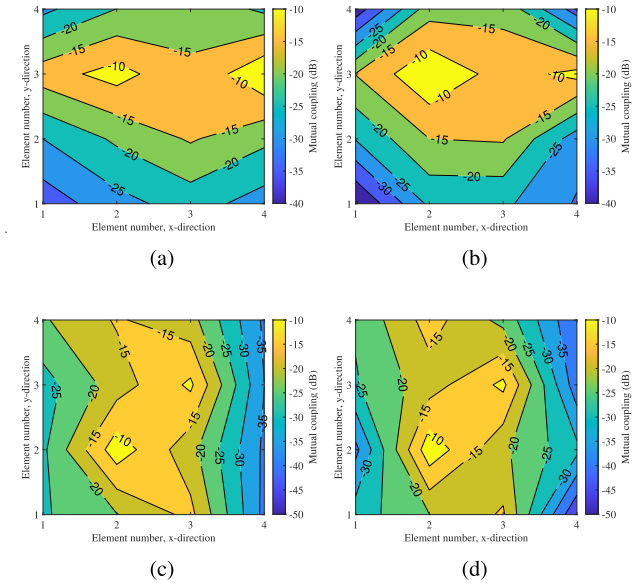

FIGURE 7. Mutual coupling between the centre element and the neighbouring elements in the finite arrays with different polarization directions and aperture geometries, the element spacing is $a = 40$ mm for the planar array, the capacitor between the adjacent elements has the capacitance value of 0.35 pF. (a) Planar array configuration of 4 × 4 array with *H/V* polarization. (b) Bent array configuration of 4 × 4 array with *H/V* polarization. (c) Planar array configuration of 4 × 4 array with slant polarization. (d) Bent array configuration of 4 × 4 array with slant polarization.

polarization at 2.5 GHz in both the planar and the curved array is shown in Fig. 7. It is noticed that in *H/V* polarizations and slant polarization, the mutual coupling between the selected port with its neighbouring ports for the array with a curvature is less distributive than in the planar counterpart. This implied that strong mutual coupling exists between nearby elements in the arrays implemented on a curved surface and it tends to spread to more elements on a planar surface with a large electrical distance between them.

The active reflection coefficient for element m at a scan angle (θ_0, φ_0) for a finite array has the following relation with the mutual coupling matrix,

$$\Gamma_{act,m}(\theta_0, \varphi_0) = \sum_{n=1}^{N} S_{m,n} e^{-jk(x_n sin\theta_0 cos\varphi_0 + y_n sin\theta_0 cos\varphi_0)} \tag{15}$$

where (x_n, y_n) is the position of element n, k is the wavenumber, and N is the total number of elements in the array. In order to calculate the active reflection coefficients for the elements in the array and evaluate the operational frequency bandwidth, the reflection coefficient of the element for observation and mutual coupling between the chosen element and the neighbouring elements of the same polarization were obtained from simulation. Then, the active reflection coefficient of the selected central element can be calculated by summing up the complex S-parameters between the element and its neighbouring elements. The simulated active reflection coefficient of an element in the 4×4 finite arrays with the unit

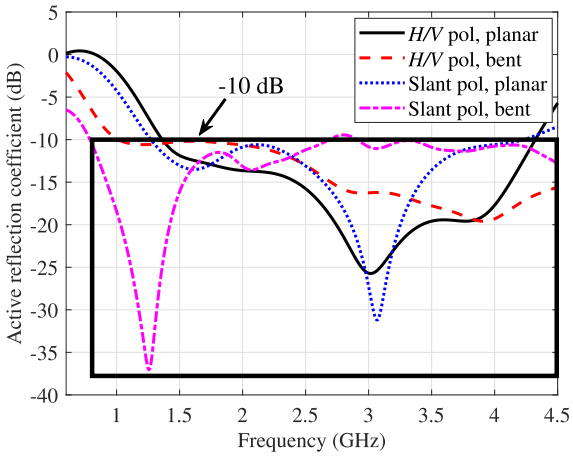

FIGURE 8. The active reflection coefficient of the elements in the finite antenna arrays with different aperture geometries.

size of 26 mm is presented in Fig. 8. It can be noted that the elements in the arrays on a curved surface exhibited a broader frequency bandwidth than on a planar surface. Meanwhile, the bandwidths of the four configurations are all over 100%.

The realized gain of the finite arrays when all elements of one polarization were excited is shown in Fig. 9. The gain values for the planar arrays are increasing approximately linearly as a function of frequency from 1.5 GHz to 4.5 GHz, and no significant difference in both polarizations are observed. In the cases when the arrays are on a curved surface, for both polarization scenarios, the gains are decreased compared with the array on a planar surface, in turn this signifies that range of scan for the arrays on a curved surface can be extended.

The radiation patterns of the four finite arrays are compared in Fig. 10 at 2.75, 3 and 4 GHz respectively. Given that the array structure is symmetric for dual polarization in all configurations, only the patterns for one polarization are displayed. For both polarization orientations, the cross polarization performance for the array on the curved surfaces degraded compared with the arrays on a planar surface. The Cross Polarization Discrimination (XPD) is greater than 20 dB for the array of slant polarization when the array was on a planar and curved surface. The beamwidth of radiation patterns for the bent array is greater than the array on a planar surface. It is noted that the direction of the boresight for the planar array is always perpendicular to the array surface whereas the peak gain direction for the array on a curved surface may deviate slightly from boresight, which is associated with the layout of elements.

More detailed performance comparison of the finite arrays with the four configurations at 2.5 and 3 GHz is summarized in Table 4. It is indicated that the frequency bandwidth of the coupling enhanced disk dipole array is over 100% in all four configurations. Gain of the finite array on a curved surface is smaller than the array on a planar surface. This is due to reduction of the array effective area in the direction of broadside caused by the bending which cause an increase in beamwidth and hence a drop in gain. Inter-port isolation, also

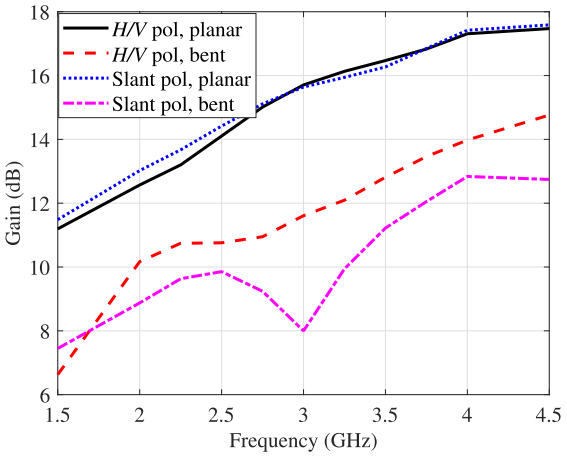

FIGURE 9. The realized gain of the antenna array at broadside when all 16 elements of x-polarization or −45° polarization were simultaneously excited with compensated time delays.

known as port-to-port isolation, is a particularly important parameter in the design of multipoint base stations as selecting antennas with high isolation reduces the complexity. For finite arrays of both the *H/V* and slant polarization, strong coupling only exists between the elements when they are physically close compared to the array on a planar surface where it exists between elements even separated by a large electrical length.

The simulated gain of antenna array of −45° polarization on the curved surface is shown in Fig. 11. At broadside, the antenna array with a greater bending angle (hence a smaller radius for bending when the aperture of the planar array is fixed) gives a wider beamwidth for the main lobe. However, the sidelobe level rose from −18 dB at broadside to −10 dB for 60° scan angle. The array beam patterns (R=100 mm, at the scan angles of 30° and 60°) denoted a similar beamwidth was produced at different scan angles. Further, the gain slightly dropped by 1.5 dB from broadside to scan at 60°.

III. THE EXPERIMENT AND RESULTS

In order to verify the performance of the finite arrays, a dual-polarized 4 × 4 finite array based on the TCDA was manufactured. The prototype was slant dual-polarized but only the elements of one polarization are integrated with the feeds as the two polarizations are in complete symmetry. The operational frequency band was designed to be between 1.0 and 4.5 GHz which covers both the key frequencies within the sub-6 GHz band for the 5G wireless communication and part of satellite communication bands. It is noted that the design principle for the array element can be easily applied to design antenna arrays operating over other higher frequency bands. Due to this scalability, the effects of curvature on the finite arrays from this analysis can be beneficial for implementing this type of arrays in many applications.

The manufactured prototype is shown in Fig. 12. To make it flexible, the metasurface was designed on a polyimide (PI) substrate with a thickness of 0.05 mm. The dual-polarized elements are printed on two sides of F_4BMX substrate having a dielectric constant of 2.55, and a thickness of 0.25 mm. The polarization directions are orthogonal to each other. The feeds are realized by bending CPWs having the same material with the antenna and a thickness of 0.762 mm, connecting the sub-miniature version A (SMA) to the feeding terminals of the balanced antenna. The rectangular ground plane is manufactured by using FR-4 material.

The active reflection coefficient of the central element in the finite array were derived based on the measured values of scattering parameters using a vector network analyser and the results were compared to simulations. The active reflection coefficient with respect to frequency when the mutual coupling effect was included is depicted in Fig. 13. It is observed that the simulation and measurement results are in a good agreement. It should be noted that although the coupling enhanced disk array was designed to operate from 1 GHz, however, due to the constraint introduced with the CPW feeds, which were necessary for the measurements, the low frequency end of the finite array with inserted CPW feed (at approximately 1.5 GHz) was higher than the array with the mutual coupled disks alone.

The realized gain and radiation patterns were measured when 16 ports of the finite array were connected to the power combiner which supports 16 ways (Talent Microwave RS16W0560-S). As shown in Fig. 13, the measured gain had a good match with the simulated results across the frequency band of interest. The discrepancy between the simulations and measurements was within 2 dB which may be attributed to the fabrication imperfection where uneven array surface was observed by the insertion of CPW feed lines.

In Fig. 14 and Fig. 15, the radiation patterns in the E-plane and H-plane at 3.75 GHz were compared between measurement and simulation. A good agreement was obtained including cross-polarization patterns despite some minor differences. It should be noted that the 3 dB beamwidth is 39° and the cross-polarized component is 17 dB below the co-polarized component in the main lobe. Insignificant discrepancy between the simulated and measured results have been observed and this may be caused by phase mismatch in the connecting cables for the power combiner. The phase differences between 16 ways of the combiner is in the range of 8° at 4 GHz.

The variation of the active reflection coefficients (indicating the impedance matching status) for the elements in the finite array when the array geometry changes is shown in Fig. 16. The size of the aperture in the direction of bending (horizontal) is 293 mm. We observed that the impedance matching slightly improved at the low end of frequency when the array was bent. The bandwidth of operation was mostly retained to a certain degree even when the radius of curvature was 75 mm, i.e., the angle of the arch formed by the array aperture is approximately 180° in the horizontal plane. This signifies that the mutual coupling enhanced disk array has a

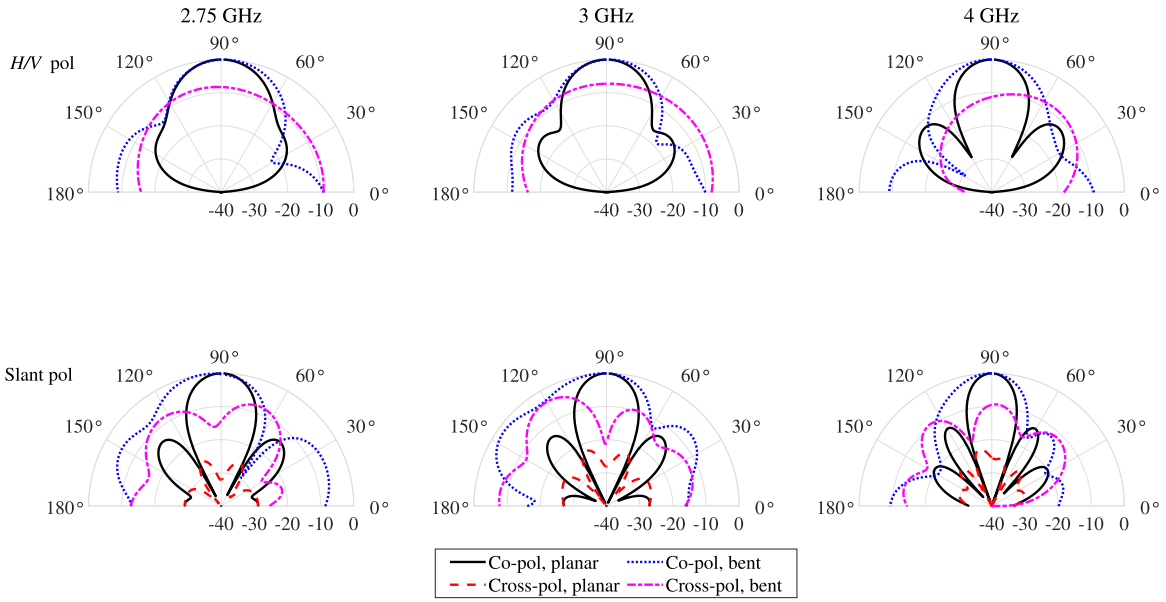

FIGURE 10. The radiation patterns of the finite arrays when all 16 elements of x-polarization or −45° polarization were simultaneously excited with time delay compensations for broadside radiation, three frequencies are shown, 2.75 GHz, 3 GHz and 4 GHz.

TABLE 4. Performance comparison of the finite arrays of four different aperture configurations based on the same type of unit cells.

Configuration	BW	Beamwidth, degree		Gain, dBi		Inter-port isolation, dB		X-pol isolation, dB		XPD, dB	
		2.5 GHz	3GHz	2.5 GHz	3GHz	2.5 GHz	3GHz	2.5 GHz	3GHz	2.5 GHz	3GHz
H/V pol, planar	104.3%	40.9	30.7	13.4	15.3	-16.8	-18.2	-40	-40.6	70.3	68.0
H/V pol, bent	134.8%	49.7	37.2	10.5	10.9	-17.2	-27.6	-38.2	-40.7	12.8	7.3
Slant pol, planar	108.1%	26.3	22.3	14.1	15.1	-18.2	-19.5	-29.2	-29.1	47.9	28.2
Slant pol, bent	140.1%	48.9	43.4	9.71	7.9	-26.9	-31.8	-23.7	-24.3	21.2	21.0

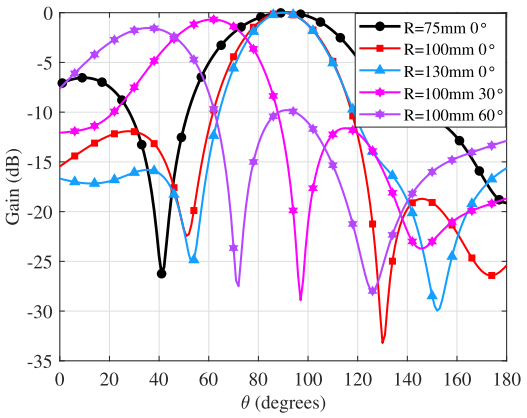

FIGURE 11. The realized gain pattern of the 4 × 4 finite array at 2.5 GHz shown in Fig. 5d when the 16 elements of one polarization, the −45° orientation, were scanned along the *x*-axis direction.

slow change on its impedance characteristics in response to deformation of the array aperture.

The performance of the bent finite array was compared to other wideband conformal arrays in the literature, and their main characteristics is summarized in Table. 5. The clear distinction of the array based on the mutual coupling enhanced crossed rings on a curved surface was demonstrated for its ultrawide bandwidth potential with only 16 elements over a limited aperture size.

IV. DISCUSSION

Antenna arrays are often designed to operate on a smooth planar surface. This places many constraints on where they can be installed particularly where a flat surface is not available. Previous work on the effect of curvature on the electromagnetic performance of antenna arrays focused on patch-like type antennas and found significant degradation in bandwidth and polarization purity, mainly due to their unbalanced structures. The effect of curvature on the electromagnetic performance of antenna arrays using a balanced tightly coupled dipole type antenna has been investigated in this study. It has been demonstrated that using this type of antenna offers a potential to achieve a broader bandwidth and higher polarization purity. This type of array antenna is entirely a balanced structure, and the effect of bending clearly showed two advantages: the beamwidth of elements became broader hence the scan range of the array was extended from the case with a uniform planar geometry; the frequency bandwidth of operation increased moderately. It is important to consider the effect of curveture on the cross polarization performance since it is an essential parameter for a wide range of applications

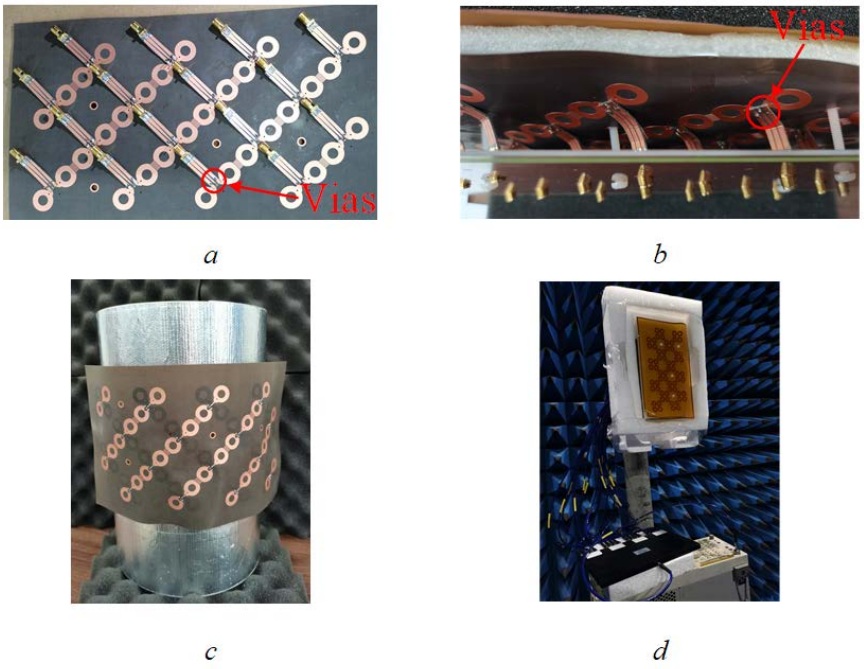

FIGURE 12. The slant dual-polarized 4 × 4 array prototype. (a) View of the CPWs for feed connected to elements in the planar array. (b) The completed prototype of the finite array in the planar configuration. (c) The finite array on the curved surface with a radius of 100 mm for studying the curvature effect, the metasurface was removed for a better view of the array elements of -45^o polarization. (d) The radiation pattern verification in the anechoic chamber.

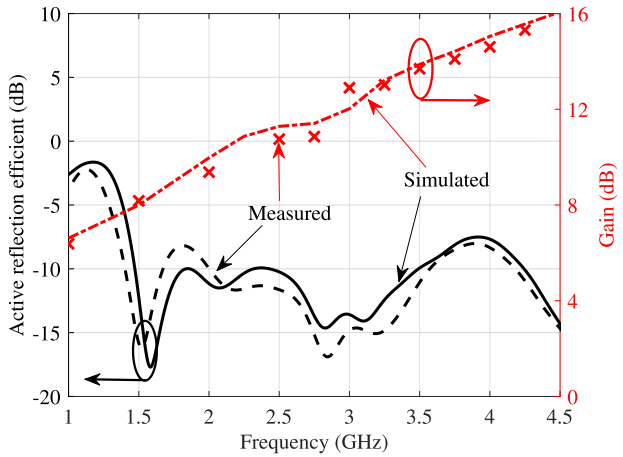

FIGURE 13. The active reflection coefficient of the element in the 4 × 4 finite array showing the largest bandwidth, and the gain when 16 elements of one polarization, −45°, were excited simultaneously, the tightly coupled disk dipole array was fed by CPWs on thin substrates.

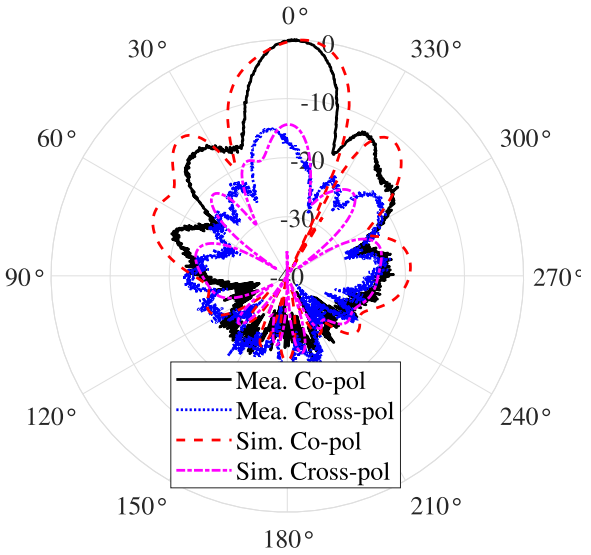

FIGURE 14. The radiation pattern at 3.75 GHz of the 4 × 4 array prototype when 16 elements of one polarization, −45°, were excited simultaneously, *E*-plane.

particularly for satellite communications. Therefore, finite arrays with different polarization orientations with respect to the axis for bending have been investigated. Despite the increased scan range achieved with bending due to a broader beam, the cross polarization performance became more complex, with the cross polarization components rising more rapidly than on a planar surface at off-boresight angles. The enhanced coupling crossed disk array demonstrated 17 dB of XPD performance in the main lobe on a curved surface over most frequency ranges. The frequency bandwidth performance of radiator elements was found to be insensitive to flatness of the surface in the mutual coupling enhanced crossed rings antenna array. This phenomenon was observed when the measurements were made on the prototype model where the array surface was made slightly uneven by insertion of

TABLE 5. Performance comparison of typical finite arrays on convex surfaces.

Finite Array	Frequency Bandwidth	Gain at f_0 (dB)	XPD (dB)	Unit cell size(λ_h)	Number of Elements
[21]	6-18 GHz (100 %)	19.1	18	$0.46 \times 0.46 \times 0.34$	64
[38]	9.5-10.5 GHz (6 %)	19.3	NA	$0.53 \times 0.53 \times 0.04$	100
[39]	8.54-11.28 GHz (27.6 %)	11.8	25	$1 \times 0.64 \times 0.2$	192
[40]	6-12 GHz (67 %)	17.52	NA	$0.48 \times 0.48 \times 0.19$	48
This work	1.5-4.5 GHz (100 %)	11.8	17	$0.48 \times 0.48 \times 0.38$	16

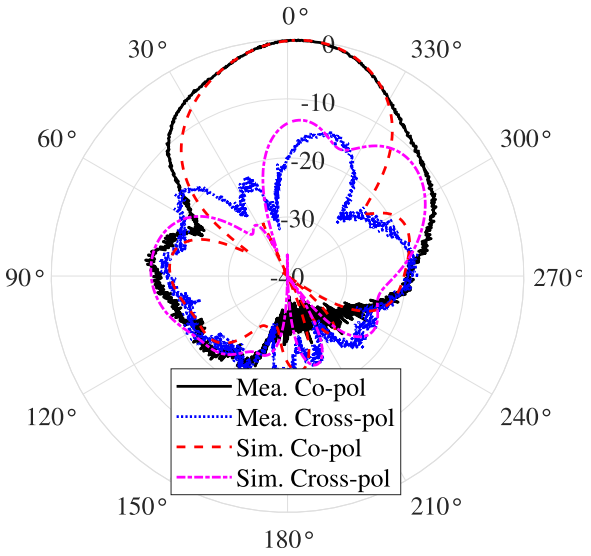

FIGURE 15. The radiation pattern at 3.75 GHz of the 4 × 4 array prototype when 16 elements of one polarization, −45°, were excited simultaneously, *H*-plane.

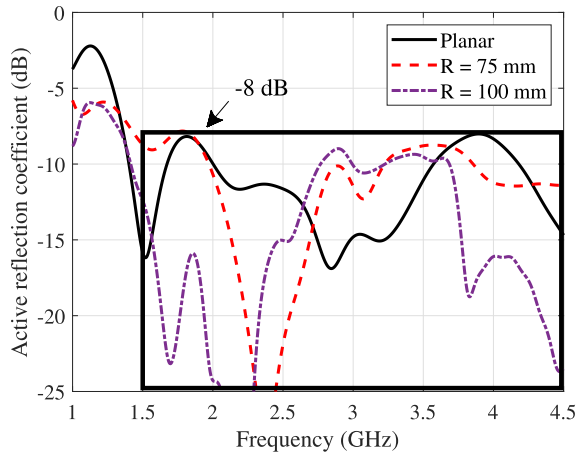

FIGURE 16. The reflection coefficients variation with deformation of the array aperture, the size of the array aperture is 270 mm in the direction for bending, the radius of the curvature for bending varied between 75 mm and 100 mm, the matching performances under the two cases are compared with the scenario of a planar configuration.

the CPW feedline for each element. The reason is related to the tight coupling between the adjacent elements for such type of arrays resulting in an insignificant effect. Ultimately, this adaptability is beneficial to realize bent arrays where tolerances needed for fabrication is less stringent in addition to more performance flexibility in final installation.

In SOTM applications, available space for installation in platforms with mobility is of high value, and the ability of the arrays to adapt to a given non-planner surface of a practical shape is crucial to minimize impact of their profiles. This investigation confirmed that the effects from curvature have the following characteristics: 1) The frequency bandwidth is largely maintained after bending and expanded further towards the low frequency end to a certain degree; 2) The scan range of the array with curvature becomes wider, thus the gain drops; 3) The polarization status change more rapidly with scan angles on a curved surface however the cross polarized component is still low at boresight; 4) the tightly coupled array antenna design differs from other previous array designs in the sense that it can adapt to conformal surfaces of different curvature radii (i.e., major instead of minor surface deformations).

V. CONCLUSION

The effect of fully curved geometry on ultrawideband finite arrays incorporating two typical dual-polarization schemes has been examined. A tightly coupled crossed ring antenna array was proposed and investigated for its foldable potential while preserving and/or even extending frequency bandwidth range which all are over 100%. The scan range of the arrays on a convex surface increased in general compared to a planar surface, in particular, and the beamwidth increased by around 20° when the elements are slant-polarized. The cross polarization performance was changed significantly on a curved surface with a more complex implication. However, it was 17 dB below the copolar component for the scan in the broadside direction. The degradation of polarization purity from effects of curvature on finite arrays can be a tradeoff with its ability to extend the scan range where a wide-angle scan is crucially a required feature for arrays in SOTM terminals on the ground. Such antenna arrays can also be used in high-speed broadband satellite service and wearable electronic devices.

ACKNOWLEDGMENT

The authors would like to express their deep gratitude to Prof. Jianxin Chen and Prof. Wenwen Yang's team for their valuable support on the antenna range testing.

REFERENCES

[1] W. Jiang, H. Zhou, M. Jong, and G. Lo, "Evolution of satellite communication antennas on mobile ground terminals," *Int. J. Antennas Propag.*, vol. 2015, pp. 436520–436533, Oct. 2015.

[2] S. Ohmori, "Phased array antennas for mobile communications," *Annales Des Télécommun.*, vol. 54, nos. 1–2, pp. 93–102, Jan. 1999.
[3] G. Han, B. Du, W. Wu, and B. Yang, "A novel hybrid phased array antenna for satellite communication on-the-move in Ku-band," *IEEE Trans. Antennas Propag.*, vol. 63, no. 4, pp. 1375–1383, Apr. 2015.
[4] H. Schippers, J. Verpoorte, P. Jorna, A. Hulzinga, A. Meijerink, C. G. H. Roeloffzen, L. Zhuang, D. A. I. Marpaung, W. van Etten, R. G. Heideman, A. Leinse, A. Borreman, M. Hoekman, and M. Wintels, "Broadband conformal phased array with optical beam forming for airborne satellite communication," in *Proc. IEEE Aerosp. Conf.*, Mar. 2008, pp. 1–17.
[5] M. Temiz, E. Alsusa, L. Danoon, and Y. Zhang, "On the impact of antenna array geometry on indoor wideband massive MIMO networks," *IEEE Trans. Antennas Propag.*, vol. 69, no. 1, pp. 406–416, Jan. 2021.
[6] A. Sattarzadeh, Y. Liu, A. Mohamed, R. Song, P. Xiao, Z. Song, H. Zhang, R. Tafazolli, and C. Niu, "Satellite-based non-terrestrial networks in 5G: Insights and challenges," *IEEE Access*, vol. 10, pp. 11274–11283, 2022.
[7] V. Weerackody and E. G. Cuevas, "Technical challenges and performance of satellite communications on-the-move systems," *Johns Hopkins APL Tech. Dig.*, vol. 30, no. 2, pp. 113–121, 2011.
[8] R. E. Anderson, R. L. Frey, J. R. Lewis, and R. T. Milton, "Satellite-aided mobile communications: Experiments, applications, and prospects," *IEEE Trans. Veh. Technol.*, vol. VT-30, no. 2, pp. 54–61, May 1981.
[9] M. H. Novak, F. A. Miranda, and J. L. Volakis, "Ultra-wideband phased array for small satellite communications," *IET Microw., Antennas Propag.*, vol. 11, no. 9, pp. 1234–1240, Jul. 2017.
[10] L. Josefsson and P. Persson, *Conformal Array Antenna Theory and Design*. Hoboken, NJ, USA: Wiley, Feb. 2006.
[11] X. Ding, Y.-F. Cheng, W. Shao, H. Li, B.-Z. Wang, and D. E. Anagnostou, "A wide-angle scanning planar phased array with pattern reconfigurable magnetic current element," *IEEE Trans. Antennas Propag.*, vol. 65, no. 3, pp. 1434–1439, Mar. 2017.
[12] A. Meredov, K. Klionovski, and A. Shamim, "Screen-printed, flexible, parasitic beam-switching millimeter-wave antenna array for wearable applications," *IEEE Open J. Antennas Propag.*, vol. 1, pp. 2–10, 2020.
[13] R. Mayo and S. Harmer, "A cost-effective modular phased array," in *Proc. IEEE Int. Symp. Phased Array Syst. Technol.*, Oct. 2013, pp. 93–96.
[14] M. R. M. Hashemi, A. C. Fikes, M. Gal-Katziri, B. Abiri, F. Bohn, A. Safaripour, M. D. Kelzenberg, E. L. Warmann, P. Espinet, N. Vaidya, E. E. Gdoutos, C. Leclerc, F. Royer, S. Pellegrino, H. A. Atwater, and A. Hajimiri, "A flexible phased array system with low areal mass density," *Nature Electron.*, vol. 2, no. 5, pp. 195–205, May 2019.
[15] D. F. M. Boada and D. C. D. Nascimento, "Including the effects of curvature in the cavity model and new manufacturing considerations for cylindrical microstrip antennas," *IEEE Antennas Wireless Propag. Lett.*, vol. 17, no. 12, pp. 2419–2423, Dec. 2018.
[16] D. M. Pozar, "Microstrip antennas," *Proc. IEEE*, vol. 80, no. 1, pp. 79–91, Jan. 1992.
[17] P. Wang, G. Wen, H. Zhang, and Y. Sun, "A wideband conformal end-fire antenna array mounted on a large conducting cylinder," *IEEE Trans. Antennas Propag.*, vol. 61, no. 9, pp. 4857–4861, Sep. 2013.
[18] X. Lv, Y. Zhang, Q. Shi, M. Temiz, and A. El-Makadema, "A dual slant-polarized cylindrical array of tightly coupled dipole antennas," *IEEE Access*, vol. 10, pp. 30858–30869, 2022.
[19] Y. Zhang, Q. Shi, A. El-Makadema, L. Danoon, and A. K. Brown, "Triangular grid interconnected crossed rings antenna for large-scale ultra-wideband dual-polarised arrays," *IET Microw., Antennas Propag.*, vol. 14, no. 15, pp. 2115–2122, Dec. 2020.
[20] H. Zhang, S. Yang, S. Xiao, Y. Chen, and S. Qu, "Low-profile, lightweight, ultra-wideband tightly coupled dipole arrays loaded with split rings," *IEEE Trans. Antennas Propag.*, vol. 67, no. 6, pp. 4257–4262, Jun. 2019.
[21] S. Xiao, S. Yang, H. Zhang, Q. Xiao, Y. Chen, and S.-W. Qu, "Practical implementation of wideband and wide-scanning cylindrically conformal phased array," *IEEE Trans. Antennas Propag.*, vol. 67, no. 8, pp. 5729–5733, Aug. 2019.
[22] J. Zhong, A. Johnson, E. A. Alwan, and J. L. Volakis, "Dual-linear polarized phased array with 9:1 bandwidth and 60° scanning off broadside," *IEEE Trans. Antennas Propag.*, vol. 67, no. 3, pp. 1996–2001, Mar. 2019.
[23] B. Munk, R. Taylor, T. Durharn, W. Croswell, B. Pigon, R. Boozer, S. Brown, M. Jones, J. Pryor, S. Ortiz, J. Rawnick, K. Krebs, M. Vanstrum, G. Gothard, and D. Wiebelt, "A low-profile broadband phased array antenna," in *Proc. IEEE Antennas Propag. Soc. Int. Symp.*, vol. 2, Jun. 2003, pp. 448–451.
[24] M. D. Huang and M. H. A. J. Herben, "Effects of bending a planar antenna array on its scan performance," in *Proc. 4th Eur. Conf. Antennas Propag. (EUCAP)*, 2010, pp. 1–5.
[25] M. C. Gonzalez, B. P. Kumar, and G. R. Branner, "Generalised design method of broadband array antennas using curved geometry," *IET Microw., Antennas Propag.*, vol. 10, no. 14, pp. 1553–1562, Nov. 2016.
[26] X. Zhang, G. Liao, Z. Yang, X. Zou, and Y. Chen, "Effective mutual coupling estimation and calibration for conformal arrays based on pattern perturbation," *IET Microw., Antennas Propag.*, vol. 14, no. 15, pp. 1998–2006, Dec. 2020.
[27] J. K. Pakkathillam and M. Kanagasabai, "Performance evaluation of a dual band paper substrate wireless sensor networks antenna over curvilinear surfaces," *IET Microw., Antennas Propag.*, vol. 9, no. 8, pp. 715–722, Jun. 2015.
[28] M. Ur-Rehman, Q. H. Abbasi, M. Akram, and C. Parini, "Design of band-notched ultra wideband antenna for indoor and wearable wireless communications," *IET Microwaves, Antennas Propag.*, vol. 9, no. 3, pp. 243–251, 2015.
[29] S. Yan, P. J. Soh, and G. A. E. Vandenbosch, "Wearable dual-band magneto-electric dipole antenna for WBAN/WLAN applications," *IEEE Trans. Antennas Propag.*, vol. 63, no. 9, pp. 4165–4169, Sep. 2015.
[30] G.-P. Gao, C. Yang, B. Hu, R.-F. Zhang, and S.-F. Wang, "A wide-bandwidth wearable all-textile PIFA with dual resonance modes for 5 GHz WLAN applications," *IEEE Trans. Antennas Propag.*, vol. 67, no. 6, pp. 4206–4211, Jun. 2019.
[31] J. Gilmore and D. B. Davidson, "Suppressing undesired common-mode resonances in connected antenna arrays," *IEEE Trans. Antennas Propag.*, vol. 63, no. 11, pp. 5245–5250, Nov. 2015.
[32] E. Yetisir, J. Li, and N. Ghalichechian, "UWB dual-polarised dipole array with dielectric and FSS superstrate and 65° scanning," *IET Microw., Antennas Propag.*, vol. 13, no. 3, pp. 313–321, Feb. 2019.
[33] J. A. Kasemodel, C.-C. Chen, and J. L. Volakis, "Wideband planar array with integrated feed and matching network for wide-angle scanning," *IEEE Trans. Antennas Propag.*, vol. 61, no. 9, pp. 4528–4537, Sep. 2013.
[34] A. D. Johnson, J. Zhong, S. Sekelsky, E. A. Alwan, and J. L. Volakis, "Dual-polarised wideband tightly coupled dipole array for airborne applications," *IET Microw., Antennas Propag.*, vol. 14, no. 12, pp. 1476–1480, Oct. 2020.
[35] X. Lv, Y. Zhang, Q. Shi, Y. Fu, H. Xing, and M. Temiz, "Dual function flexible coplanar waveguide for feeding antenna of balanced structure," in *Proc. 13th Int. Symp. Antennas, Propag. EM Theory (ISAPE)*, vol. 1, Dec. 2021, pp. 1–3.
[36] C. A. Balanis, *Antenna Theory Analysis and Design*, 4th ed. Hoboken, NJ, USA: Wiley, 2016, ch. 8, pp. 458–480.
[37] A. D. Brown, *Electronically Scanned Arrays: MATLAB Modeling and Simulation*, 1st ed. Boca Raton, FL, USA: CRC Press, 2012, ch. 1, pp. 19–22.
[38] Y. Liu, H. Yang, Z. Jin, F. Zhao, and J. Zhu, "A multibeam cylindrically conformal slot array antenna based on a modified Rotman lens," *IEEE Trans. Antennas Propag.*, vol. 66, no. 7, pp. 3441–3452, Jul. 2018.
[39] D. Sun, W. Dou, and L. You, "Application of novel cavity-backed proximity-coupled microstrip patch antenna to design broadband conformal phased array," *IEEE Antennas Wireless Propag. Lett.*, vol. 9, pp. 1010–1013, 2010.
[40] S. Hussain, S.-W. Qu, P. Zhang, X.-H. Wang, and S. Yang, "A low-profile, wide-scan, cylindrically conformal X-band phased array," *IEEE Antennas Wireless Propag. Lett.*, vol. 20, no. 8, pp. 1503–1507, Aug. 2021.

YANWEI FU received the B.S. degree in electronic engineering from Nantong University, Nantong, Jiangsu, China, in 2021, where she is currently pursuing the M.S. degree with the School of Transportation. Her research interests include electromagnetic theories, metamaterial characterization, and conformal antenna arrays.

YONGWEI ZHANG (Member, IEEE) received the B.S. degree in communication engineering from Jilin University, in 1996, and the Ph.D. degree from the School of Electrical and Electronic Engineering, The University of Manchester, U.K., in 2007.

In 1996, he joined Lucent Technologies (AT&T initially), China, where he was an Application Engineer on 5ESS® system, and later a System Engineer and had been worked with Lucent, until 2003. While he was working with Lucent, in 1998, he was sent as a Visitor to the Bell Laboratories, Indian Hill, Naperville, IL, USA, trained in communication system engineering tool development and later certified as an International Instructor. In the years working with Lucent Technologies, from 1996 to 2003, he had been involved in 5ESS® switch application engineering and optimization for wireless communication systems. In 2003, he joined The University of Manchester first as a Ph.D. Student and later as a Research Fellow, then the Task Leader of the front-end design work package in Mid-Frequency Aperture Array Consortium for the Square Kilometre Array (SKA). His current research interests include antenna and array designs based on flexible material, electromagnetic theories, antenna array calibration techniques, and radio astronomy instrumentation. In 2000, he was awarded as an Outstanding Member of the PHS Project Team. He received the Lucent (China) Chairman Award in 2001.

QUAN SHI received the M.S. and Ph.D. degrees in management information systems from the University of Shanghai for Science and Technology, Shanghai, China, in 2005 and 2011, respectively.

He is currently the Head of the School of Transportation and Civil Engineering, Nantong University, China. His research interests include signal and image processing in intelligent transportation systems and big data techniques.

MURAT TEMIZ (Member, IEEE) received the B.S. degree from Gazi University, Ankara, Turkey, in 2011, the M.S. degree from the TOBB University of Economics and Technology, Ankara, in 2013, and the Ph.D. degree from the School of Electrical and Electronic Engineering, The University of Manchester, Manchester, U.K., in 2020.

Since 2013, he has been with the Department of Electrical and Electronic Engineering, The University of Manchester, where he is also working as a Research Assistant focusing on massive multiple-input–multiple-output (MIMO) communication, MIMO orthogonal frequency-division multiplexing (OFDM) radars, and developing energy efficiency improvement methods for such systems. His current research interests include massive MIMO systems, antenna array design, channel measurements, array geometry optimization, dual-functional MIMO OFDM radar communication systems, and machine learning application in electromagnetic.

AHMED EL-MAKADEMA received the B.S. degree in computing and communication systems engineering, the M.S. degree in communication engineering, and the Ph.D. degree in microwave and communication systems from The University of Manchester, in 2004, 2005, and 2011, respectively.

He has been a member of the team working on the Square Kilometre Array (SKA) Project, since 2006. His research interests include ultrawideband antenna, low-cost large antenna array geometry optimization, conformal antenna arrays, beamforming techniques, and electromagnetic computation.

JIAJIA SHI (Member, IEEE) received the B.Sc. and M.E. degrees from Central South University, Changsha, China, in 2007 and 2010, respectively, and the Ph.D. degree from the University of Technology Sydney, Ultimo, NSW, Australia, in 2015. He is currently an Associate Professor with the School of Transportation and Civil Engineering, Nantong University, Nantong, China. His research interests include signal processing and electronics.